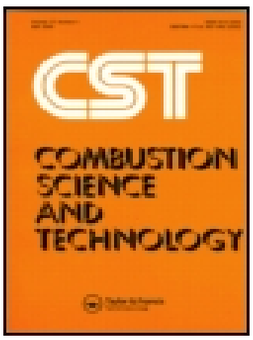

Taylor & Francis
Taylor & Francis Group

Combustion Science and Technology

ISSN: 0010-2202 (Print) 1563-521X (Online) Journal homepage: http://www.tandfonline.com/loi/gcst20

Pyrolysis and Combustion of Regional Agro-Industrial Wastes: Thermal Behavior and Kinetic Parameters Comparison

Anabel Fernandez, Carlos Palacios, Marcelo Echegaray, German Mazza & Rosa Rodriguez

To cite this article: Anabel Fernandez, Carlos Palacios, Marcelo Echegaray, German Mazza & Rosa Rodriguez (2017): Pyrolysis and Combustion of Regional Agro-Industrial Wastes: Thermal Behavior and Kinetic Parameters Comparison, Combustion Science and Technology, DOI: 10.1080/00102202.2017.1377701

To link to this article: http://dx.doi.org/10.1080/00102202.2017.1377701

Accepted author version posted online: 08 Sep 2017.
Published online: 08 Sep 2017.

COMBUSTION SCIENCE AND TECHNOLOGY
https://doi.org/10.1080/00102202.2017.1377701

Taylor & Francis
Taylor & Francis Group

Pyrolysis and Combustion of Regional Agro-Industrial Wastes: Thermal Behavior and Kinetic Parameters Comparison

Anabel Fernandez[a], Carlos Palacios[a], Marcelo Echegaray[a], German Mazza[b], and Rosa Rodriguez[a]

[a]Instituto de Ingeniería Química, Facultad de Ingeniería, Universidad Nacional de San Juan, Libertador, Argentina; [b]Instituto de Investigación y Desarrollo en Ingeniería de Procesos, Biotecnología y Energías Alternativas, CONICET-Universidad Nacional del Comahue, Neuquén, Argentina

ABSTRACT

The thermal decomposition of six regional agro-industrial wastes under inert and oxidative atmosphere at different heating rates was studied using thermogravimetric analysis. The kinetic parameters were calculated using the DAEM (distributed activation energy model) and FWO (Flynn–Wall–Ozawa) methods. The obtained thermogravimetric and differential thermogravimetric curves show similar shapes, considering the pyrolysis and combustion phenomena. Nevertheless, the biomass weight loss is slower and smaller under inert than oxidative atmosphere. The activation energy average values (*E*) in inert atmosphere for the active pyrolysis stage is about 133.90–275.57 kJ/mol and 136.51–261.10 kJ/mol for DAEM and FWO, respectively. The *E* average values for the devolatilization stage under oxidative atmosphere are about 104.11–125.73 kJ/mol and 108.40–128.81 kJ/mol using DAEM and FWO methods, respectively. The results calculated by FWO and DAEM methods show differences between activation energies for the same waste below 8%; thus, they were reliable and predictive in this study. The variation of *E* values with progressing conversion for two studied processes indicated the existence of a complex multi-step mechanism that occurs during the degradation process. Moreover, during the devolatilization stage of combustion, the lower value of *E* indicates that the combustion is produced in parallel to pyrolysis; the oxygen reacts with the remaining solid.

ARTICLE HISTORY
Received 21 January 2017
Revised 2 August 2017
Accepted 5 September 2017

KEYWORDS
DAEM and FWO models; Regional agro-industrial wastes; Thermogravimetric analysis; Thermal decomposition

Introduction

The decrease in reserves of fossil fuel and the increase of energy demand have raised the need to find different substitutes. There is considerable interest concerning biomass as a renewable energy source in the context of climate change, mitigation, and energy security. Considering that the principal economic activity of Argentina is agroindustry, biomass wastes conversion through thermal treatment could be advantageous due to the wide availability of this source. There are different processes in order to convert biomass in energy, one being thermochemical conversion, which is one of more important technologies. Pyrolysis, gasification, and combustion are some of the main thermochemical conversion routes and promising constituents of a future renewable energy scenario. In order to design and simulate the thermochemical processes reactors, it is necessary to

CONTACT Rosa Rodriguez rrodi@unsj.edu.ar Instituto de Ingeniería Química, Libertador 1109 (O), San Juan 5400, Argentina.

Color versions of one or more of the figures in the article can be found online at www.tandfonline.com/gcst.

propose reliable comprehensive models that achieve a better understanding of the chemical reactions in each process (Sanchez-Silva et al., 2013).

In addition, several species have been investigated for the thermochemical conversion processes, and their kinetic parameters and decomposition characteristics have been determined using thermogravimetric analysis (Jerguirim and Trouvé, 2009; Meszaros et al., 2004). In the present literature, there are also studies on the influence and interaction between the main characteristics of biomasses that can be used as raw materials for energy production (Senelwa and Sims, 1999).

The use of biomass for energy purposes allows the development of new activities based on a market with continuous demand and without fluctuations, which generates stable, well-paid jobs and represents a new source of income for local industries. According to the Committee of the Regions in its opinion on the White Paper on Renewable Energies (Department of Minerals and Energy, 2003), up to five times more jobs are created with renewable energy than with conventional fuels (Mitchell and Connor, 2004).

On the other hand, the contribution to a smaller external dependence of the supply of fuels, also facilitating the rural development, is one of the most outstanding macroeconomic bases of the energy coming from the biomass. The use of biomass in single-family heating, centralized heating of buildings, or in centralized heating networks are viable alternatives to the consumption of natural gas and other fossil fuels, and can be favored and expanded if standards are developed that promote and encourage their implementation at local, regional, and national levels (Ericsson and Werner, 2016).

In view of the Cuyo Region, Argentina, one of the most important economic activities is the agro-industry, highlighting the wine, olive, wood, and seasonal fruits industries, such as peaches and plum. This sector produces a significant environmental impact in specific geographical areas. In this country, approximately $1.40 * 10^5$ t of peaches and plums are processed in the canning and jam industries, generating an important solid biomass wastes quantity, $7.98 * 10^4$ t/year. A quantity of marc and stalk equal to $5.19 * 10^4$ t/year is generated by the wine industry. About $1.5 * 10^5$ t/year of olive oil is produced, generating $7 * 10^5$ t/year of olive pits. Finally, the wood industry produces approximately $7 * 10^3$ t/year of sawdust (INTA, 2015).

These wastes are lignocellulosic biomass with relatively low moisture contents and they are appropriate to obtain energy using the thermal treatment. In order to exploit these wastes to obtain steam and after electricity, a combustor was installed in this region. Nevertheless, much of this potential is unused in spite of the environmental advantages and the economic benefits of this source of energy because there are some problems in current biomass combustion reactors. In this case, the following problems were observed: lower thermal efficiency than fossil gas (the biomass has a minor heating value); instability of heat load due to the variability of different used biomass with a wide moisture content; slagging production (several biomass have a high K and Cl content). These problems, have to be improved to avoid the irrational use of biomass (Prasad et al., 2014).

Like other types of lignocellulosic biomass, agro-industrial waste mainly contains cellulose, hemicellulose, and lignin. Therefore, high value added biofuel or heat can be generated from the pyrolysis and combustion of agro-industrial wastes (Gao et al., 2013). Pyrolysis is a thermally assisted decomposition process in the absence of oxygen, during which lignocellulosic biomass can be converted into syngas, bio-oil, and bio-char (Dufour et al., 2013; Jahirul et al., 2012; Mettler et al., 2012). Syngas and bio-oil have higher heating

values (HHV) and can be used for energy recovery. Bio-oil can also be further upgraded into renewable transportation fuels to replace gasoline, diesel, and chemicals currently derived from nonrenewable sources (Carlson et al., 2011; Carpenter et al., 2014; Paulsen et al., 2014; Talmadge et al., 2014; Zhang et al., 2013). Bio-char can be used as a fuel (Abdullah and Wu, 2009), activated carbon (Jung et al., 2013), or as a fertilizer replacement, offering an advanced option for biological sequestration of carbon (Ahmad et al., 2014; Lehmann, 2007; Manya, 2012). Combustion of agro-industrial wastes can be used for electrical and heat energy (Nunes et al., 2017). An example of this use is the combustor installed in the Cuyo region, as previously described.

Thermoanalytical techniques, in particular thermogravimetric analysis (TGA) and derivative thermogravimetry (DTG), permit researchers to find the information about thermal processes in a simple and straightforward way. TGA is one of the more commonly adopted techniques to study thermal events during the thermal process (Aouad et al., 2002; Borah et al., 2005; Kök, 1998, 2003; Kök and Pamir, 2003b; Kök and Karacan, 1998).

The pyrolysis and combustion kinetics can help to produce sub-models that can be coupled with transport phenomena to describe practical conversion processes and design more efficient reactors (Cai et al., 2014). In previous studies (Fernandez et al., 2016, 2017), the kinetic analysis was developed using Coats–Redfern and Sharp methods. These model fittings permitted us to determine the most probable reaction mechanism for the agro-industrial wastes studied in the present work at different decomposition atmospheres. The models found contraction geometry for the pyrolysis active and the devolatilization stages, and the first-order reaction model for the char combustion stage. Nevertheless, the involved reactions in the pyrolysis and combustion of agro-industrial wastes are very complex and the corresponding activation energies may vary with the degree of conversion. In this point, it is important to note that the isoconversional methods are strongly recommended to determine the activation energy, and assist in the first guess for the more complex kinetic schemes (Vyazovkin et al., 2011). The variation of the activation energies can be obtained by means of isoconversional kinetic methods and the distributed activation energy model (DAEM; Wang et al., 2016). The first methods yield the effective activation energies as a function of the degree of conversion and permit to draw reliable mechanistic conclusions (Venkatesh et al., 2013). The Flynn–Wall–Ozawa (FWO) method is one of the most commonly accepted model-free techniques. The essential assumption of the first method is that the reaction rate for a constant extent of conversion (α) depends only on the temperature (T). Alternatively, DAEM is a multi-reaction model; it assumes that many decomposition nth order reactions with distributed activation energies occur simultaneously. In this case, a parallel reaction model is assumed. The distribution of reactivity resulting from the reaction complexity is represented with enough reliability by a series of independent, parallel reactions, each of them with its own activation energy and frequency factor (Vand, 1943).

Materials and methods

Solid biomass wastes characterization

Samples preparation

The samples were collected from the wastes of canneries, jam industries, wineries, and the timber industry, which are located in San Juan province, Argentine. There are about six kinds of lignocellulosic biomasses: peach, plum, and olive pits; marc, stalk, and sawdust.

These materials were ground and sieved, and the resulting 0.10–0.21-mm size fraction was used for the TGA. The samples were dried at 333 K to constant weight in a stove.

Proximate and ultimate analysis

The moisture, ash, and organic matter content were determined according to ASTM standards (ASTM D3173-87; ASTM D3172-89). Elemental analysis of the samples was performed using a EuroEA3000 elemental analyzer. In order to calculate the HHV, the correlation proposed by Channiwala and Parikh (2002) was used (Table 1):

$$HHV\ [MJ/Kg] = 0.3491C + \ 1.1783H + 0.1005S - 0.1034O - 0.0151N - 0.0211A \quad (1)$$

where *C, H, S, O, N*, and *A* are the content of carbon (percentage on weight), hydrogen, sulfur, oxygen, nitrogen, and ash in the biomass, respectively.

Thermogravimetric analysis

A series of non-isothermal experiments was conducted for TGA using a microbalance (TGA-50, Shimadzu, North America). The used heating rate was equal to 5 K/min, 10 K/min, and 15 K/min; the temperature range was 302–1173 K. The sample was placed in microbalance at room temperature; hence, the TGA temperature was increased to 302 K while the sample was sitting in a pan and data were recorded from that temperature. A graphic of used equipment is shown in Figure 1. Figure 2 shows the temperature profile during the experiences. Approximately 12 mg of agro-industrial wastes samples were placed in the equipment. The selected particles' size minimized heat transfer phenomenon limitations, affecting the reactions when the particle size is greater than 2 mm (Abed et al., 2012; Volpe et al., 2017). However, the mass transfer phenomena are always present causing secondary reactions to occur. Hence, the model proposed is valid for the particular set of analyses conducted and they give valuable insight. The inert gas used for pyrolysis was nitrogen with a flow rate of 100 mL/min. On the other hand, to simulate the combustion, the composition of the used atmosphere was: 79% nitrogen and 21% oxygen with a flow rate equal to 100 mL/min. For each agro-industrial waste and heating rate, three replications were performed. The reproducibility of the experiments was acceptable with an error less than 5%.

Table 1. Results of proximate and ultimate analysis (dry basis, wt%).

	Peach pits	Stalk	Marc	Plum pits	Olive pits	Sawdust
C	53.01	46.14	52.91	48.95	52.79	44.71
H	5.90	5.74	5.93	1.38	2.57	1.48
N	2.32	6.37	5.41	0.99	1.39	4.20
S	1.88	4.21	5.34	0.27	0.50	0.28
O*	36.89	37.54	30.41	48.41	42.75	49.33
Ash	1.30	10.16	8.81	0.73	2.33	1.19
Volatile matter (as received)	79.10	55.84	68.60	77.86	77.25	80.90
Fixed carbon	13.90	23.07	21.98	15.55	15.87	11.06
Moisture content (as received)	5.70	7.70	8.38	5.86	4.55	6.85
HHV (MJ/Kg)	21.39	12.03	13.31	13.71	17.02	12.19

Note. High heating values (HHV; dry basis).
*By difference.

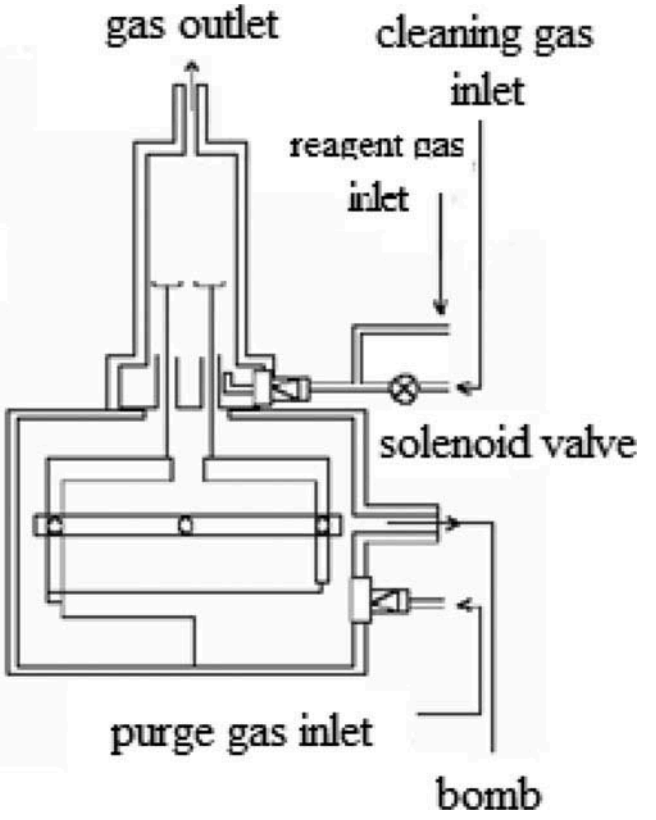

Figure 1. Graphic of used TGA equipment.

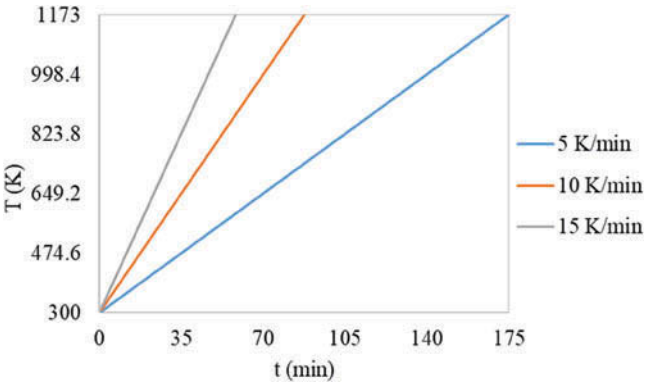

Figure 2. Temperature profile during the experiences in oxidative and inert atmosphere.

Kinetic analysis

The basic rate equation applied in all kinetic studies is described by Eq. (2):

$$\frac{d\alpha}{dt} = k(T)f(\alpha) \tag{2}$$

where t, α, $d\alpha/dt$, $f(\alpha)$, and K are time, conversion degree or extent of reaction, the process rate, conversion function, and rate constant, respectively. The conversion function represents the reaction model used and depends on the controlling mechanism. The extent of reaction α can be defined as the mass fraction of biomass substrate that has decomposed and can be expressed as shown below:

$$\alpha = \frac{w_{0-}w}{w_{0-}w_f} \tag{3}$$

where w, w_0, and w_f are the mass present at any time t, the initial mass, and the final mass of solids remaining after the reaction, respectively. The temperature dependence rate constant is expressed in terms of the Arrhenius equation as in Eq. (4):

$$\frac{d\alpha}{dt} = A\ e^{\frac{-E}{RT}} f(\alpha) \tag{4}$$

where A is pre-exponential factor; E is activation energy; R is gas constant; T is absolute temperature; and $f(\alpha)$ is reaction model.

At a constant linear heating rate, $\beta = dT/dt$, integrating Eq. (4) by separation of variables gives:

$$g(\alpha) = \int_0^{\alpha} \frac{d\alpha}{f(\alpha)} = \frac{A}{\beta}\int_{T_0}^{T} e^{-\frac{E}{RT}} dT \tag{5}$$

Letting $x = -E/RT$, Eq. (5) becomes:

$$g(\alpha) = \frac{AE}{\beta R}\left[-\frac{e^x}{x} + \int_o^{\infty}\frac{e^x}{x}dx\right] = \frac{AE}{\beta R}\ p(x) \tag{6}$$

The term $p(x)$ is the temperature integral and has no exact analytical solution. Therefore, only numerical integration or approximations can be used to solve the complex integral. The difference of different iso-conversional methods is the type of applied approximation. In this study, two approximations adopted to solve this equation are explained in the following section.

Flynn–Wall–Ozawa (FWO) method

The FWO is one the most commonly accepted model-free techniques for the determination of kinetic parameters. The temperature integral in Eq. (6) was linearized using Doyle's empirical approximation (Doyle, 1961) described in Eq. (7):

$$\ln P(x) \cong -5.331 - 1.052x \tag{7}$$

The final form of the FWO equation is expressed below:

$$ln\beta = ln\frac{AE}{Rg(\alpha)} - 5.331 - 1.052\frac{E}{RT} \tag{8}$$

Thus, a linear plot of $ln\beta$ versus $1/T$ can be used to evaluate the activation energy corresponding to each conversion step.

Distributed activation energy model (DAEM) method

The distributed activation energy model belongs to multi-reaction models. The basic assumption of DAEM is that infinity irreversible parallel first-order reactions are produced and they occur simultaneously. In this model, the activation energy usually follows a Gauss distribution profile. This model has been extensively used for analyzing the complex reactions occurring during the thermal decomposition of fossil fuels. On the other hand, according to Fiori et al. (2012), DAEM is appropriate to describe the thermal decomposition of biomass wastes. It assumes that the irreversible first-order reactions have different kinetic parameters. Based on Lili et al. (2013), E and A can be calculated by the following equation:

$$ln\frac{\beta}{T^2} = ln\frac{RA}{E} + 0.6075 - \frac{E}{RT} \tag{9}$$

Equation (9) develops a linear relationship between $ln\frac{\beta}{T^2}$ and $1/T$ with the slope of $(-E/R)$. Both activation energy E and frequency factor A can be determined from the slope and intercept of the Arrhenius plots.

Result and discussion

Characterization of the raw material

Taking into account the obtained results of ultimate analysis shown in Table 1, the C content varies between 44.71% and 53.01% for all studied regional agro-industrial wastes. It is important to note that the biomass shows a higher O and H content than the fossil fuels. Thus, the following covalent bonds contribute to HHV in decreasing order: C=C, S–H, C–H, C–C, C–N, N–H, C=O, C–O, and O–H (Lestander and Rhén, 2005). As can be seen, high O and H contents produce a smaller HHV due to the smaller contained energy in C–H, C–O, and O–H bonds compared with the C=C and C–C bonds. On the other hand, Volpe et al. (2016) carried out pyrolysis experiments using grape marc under nitrogen atmosphere. They observed that H is related to C by its reactivity in char, so when H is released, C becomes more stable due to C–C becoming more aromatic.

The N and S contents in the studied biomass wastes are between 1.38–6.37% and 0.27–5.34%, respectively. Taking into account the founded low contents of these elements, the pollutant compounds released, such as SO_x and NO_x, will be negligible. The results shown in Table 1 are consistent with those reported by Biney et al. (2015) in sawdust; reported by Valente et al. (2015) in stalk; and reported by Bhavanam and Sastry (2014) in cotton husk.

The proximate analysis results are shown in Table 1. The marc shows the highest moisture content and the olive pits show the smallest. It is necessary to consider that a smaller water content decreases the energy requirements to carry out the thermal treatment, reduce the residence time for drying, and rises the temperature resulting in better conversion of the hydrocarbons. According the obtained results, the stalk shows the highest ash content, affecting undesirably its thermal conversion.

The obtained values of HHV for the six agro-industrial wastes are similar to those reported by Demirbas and Arin (2002) and Quirino et al. (2005). The peach pits show the highest HHV due to the high content of carbon.

Related to the volatile contents, the obtained values, 55.84–80.90 wt%, are comparable to the results reported by Jeguirim and Trouvé (2009)—68.4 wt%, Daouk et al. (2015)—83.3 wt%, approximately, and Crnkovic et al. (2012)—79.7–98.6 wt%. For fixed carbon, it was observed that the results of Jeguirim and Trouvé (2009)—18.4 wt% and Daouk et al. (2015)—15.4 wt%, approximately, are similar to the obtained values in this work (between 11.06% and 23.07%, dry basis). According to the correlation proposed by Parikh et al. (2005) to calculate the HHV of solid fuels, considering the proximate analysis, the higher volatile matter/fixed carbon ratio improves the contact of reactants and reduces the residence time for the combustion process. That is, if the biomass has higher volatiles content it reacts thermochemically at lower temperatures. The stalk shows the lowest value of this ratio. On the other hand, according to Volpe et al. (2016), and comparing the difference between C and FC contents and it relation with the HHV, the peach pits should present the highest HHV value and the stalk the lowest. This prediction was confirmed in this work. The high content of organic matter makes these wastes very suitable for thermal treatment (Demirbas, 2004).

TG and DTG of regional agro-industrial wastes: Effect of heating rate and reaction atmosphere

Figures 3 and 4 show the influence of heating rate in TGA and DTG curves under inert and oxidative atmospheres (Fernandez et al., 2016, 2017). During the pyrolysis decomposition, three stages can be observed: a first drop in biomass weight is due to the moisture and light volatile releases (below 473 K), the second stage in which the decomposition of the agro-industrial wastes mainly happened (active pyrolysis), and the last stage called passive pyrolysis (Figure 3). This step is produced at high temperature and the weight loss is small (15%). Still, there remained little residue at 1173 K, i.e., about 20% of original weight.

The active pyrolysis of all solid wastes is produced between 460 K and 700 K, for 5 K/min, 10 K/min, and 15 K/min, respectively. The weight loss in this step is about 35–40% of total weight (dry basis). Chouchene et al. (2010) studied the olive solid waste thermal degradation under nitrogen atmosphere (with different oxygen concentrations) and measured the molar fraction of carbon oxides. This researcher observed that a large amount of gas species, such as CO_2, CO, CH_4, and H_2O, are released in this stage, indicating that they mainly come from this step.

At this stage, the biomass is completely dried, and its main components (hemicellulose, cellulose, and lignin) are decomposed with the temperature increasing. During this stage, gaseous compounds are released; a fraction of them are condensable and they form the liquid fraction produced during this phenomenon (Di Blasi, 2008).

During the oxidative decomposition, four stages can be observed: drying and light volatile release, devolatilization, char combustion, and residual combustion (Figure 4). These stages are associated with the peaks in the DTG curves and thus with the changes of the slopes of the TG curves. Most weight loss occurs in the devolatilization stage, giving average values equal to 56%, 55%, 54%, 42%, 45%, and 43% for peach, olive, and plum pits, stalk, marc, and sawdust, respectively. Comparing the weight loss rate for the studied wastes during this stage, the sawdust showed the highest value of this parameter at all

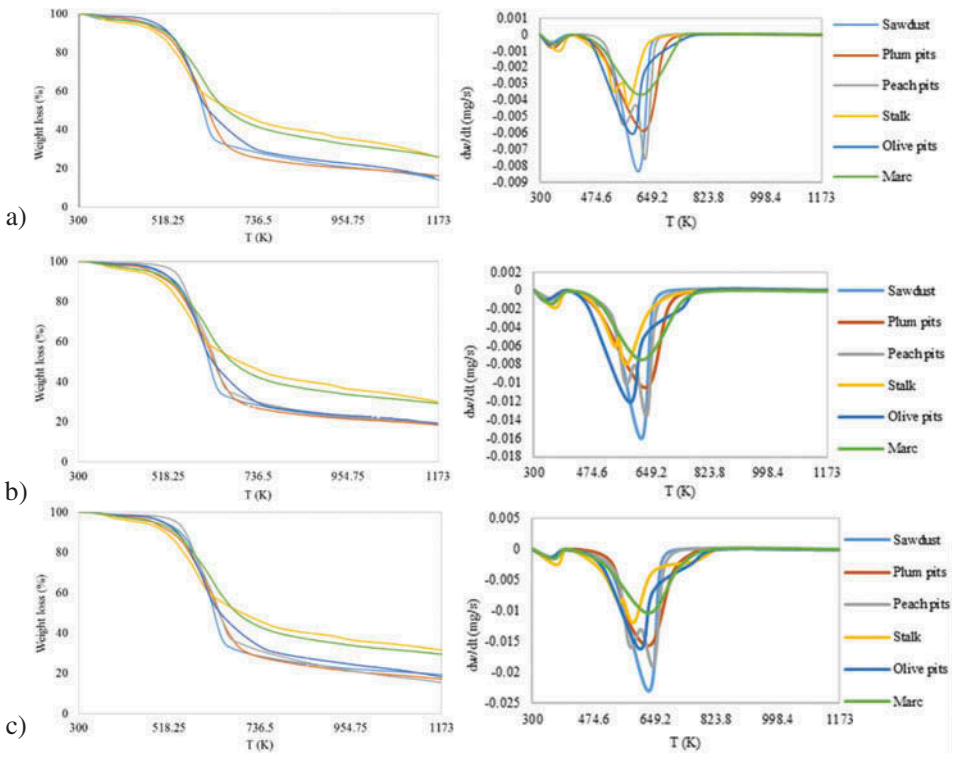

Figure 3. TG and DTG curves for the studied biomass samples at: (a) 5 K/min, (b) 10 K/min, and (c) 15 K/min under inert atmosphere.

heating rates and the marc showed the lowest value. The temperature for the maximum decomposition rate in this stage depends on the agro-industrial waste composition.

In the course of the oxidative decomposition, during the char combustion stage, occurs a high weight loss: 25%, 29%, 27%, 31%, 38%, and 23% for peach, olive, and plum pits, stalk, marc, and sawdust, respectively (average values). Zheng and Kozi (2000) studied the possible events during thermal decomposition of biomass wastes in oxidative atmosphere by TGA. Theses authors concluded that when the temperature increases during the heating phase, the evolution of different products or groups of products occurs in segmented (but overlapping) phases. During the first stage (T < 393 K), the moisture evolution is produced, then (393 K < T < 723 K) the gases release occurs, primarily CO_2 and CH_4, and later (723 K < T < 873 K) it is connected with the release of chemically bonded CO_2 and chemically formed H_2O. At temperatures higher than 873 K, species such as carbon oxides, tars, and hydrocarbon gases (heavy hydrocarbons such as fluorene, phenanthrene, fluoranthene, and benzo (a) pyrene) were identified in the gas phase. At higher temperatures, carbon oxides are the primary products. The characteristics of the agro-industrial wastes in their work are comparable with the samples used in the present research; therefore, the behavior of each stage is similar.

Under inert and oxidative atmospheres, the obtained TGA curves show different behavior, concerning temperature ranges at the same heating rate. The initial and last temperatures of each stage vary with respect to the atmosphere for the six biomass. The

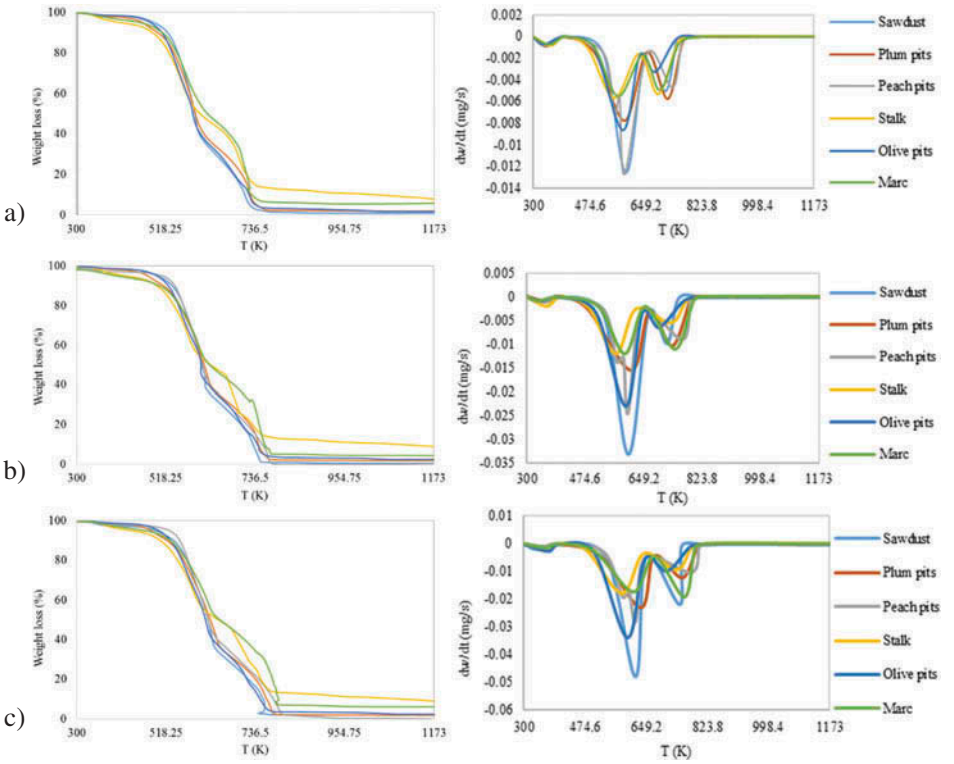

Figure 4. TG and DTG curves for the studied biomass samples at: (a) 5 K/min, (b) 10 K/min, and (c) 15 K/min under oxidative atmosphere.

differences for all agro-industrial wastes' behaviors can be related to variations of their compositions (Yang et al., 2007). According to George et al. (2014), these behaviors can be due to interrelated phenomena as the interlinking of natural biopolymers of different biomass components, the diverse thermal decomposition temperature ranges of cellulose, lignins, and hemicelluloses, and the differences between the thermal sensitivities of tars.

Considering the temperature where weight loss first reached 0.5 mg (dry basis)/min, the temperature where the weight loss reached its maximum, and the temperature where the weight loss fell below 0.5 mg/min, it is observed that the temperature range of the different decomposition stages is not affected by the heating rate. It is important to note that the limit of 0.5 mg (dry basis)/min was established as an arbitrary limit for the start and end for peaks. Figure 5 shows this behavior for the peach pits.

In all studied cases, for 15 K/min there was a lower peak temperature than that registered for 10 K/min and 5 K/min. This phenomenon is due to a longer time, which is required for the gas to reach equilibrium with the reactor temperature or particles sample as a result of the heat transfer restrictions (Abed et al., 2012). However, the weight loss is not affected when the heating rate is varied (Volpe et al., 2017).

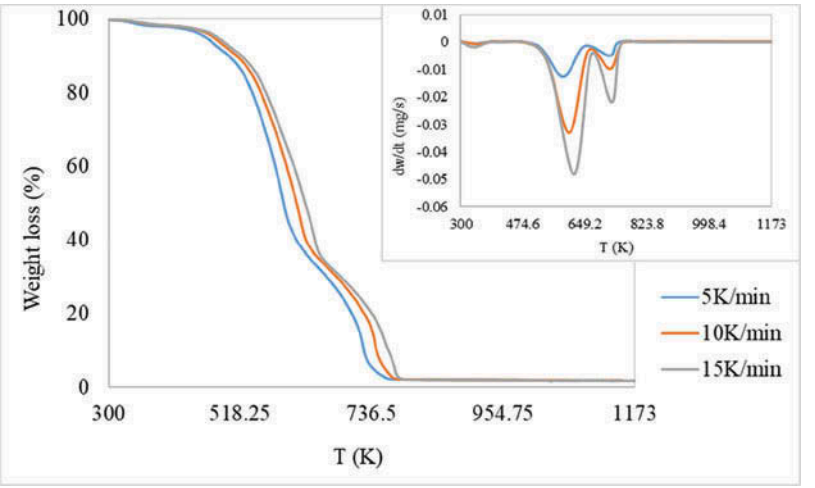

Figure 5. Comparison of the weight loss rates for peach pits under oxidative atmosphere.

Figure 6 shows the effect of atmosphere on the thermal decomposition of studied agro-industrial wastes. The shapes of TG curves of the six materials for pyrolysis are similar to those for combustion. However, the biomass weight loss is faster and higher under oxidative atmosphere than under inert atmosphere. During the decomposition under oxidative atmosphere, the maximum weight loss occurs in two steps: devolatilization and char combustion. According to Grammelis et al. (2009) and Tang et al. (2011), this phenomenon happens due to the acceleration in reaction biomass activity because there is oxygen availability.

Different amounts of final weight were obtained under inert and oxidative atmosphere.

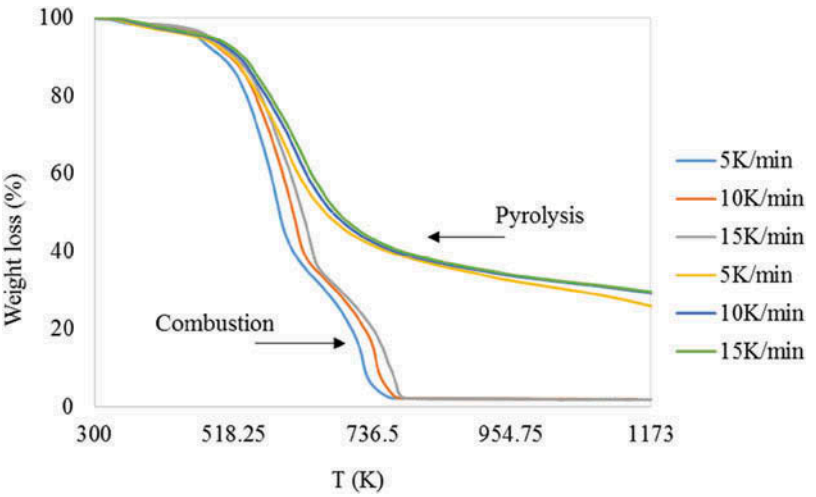

Figure 6. TGA curves at different heating rates of the pyrolysis and combustion for marc.

Pyrolysis and combustion kinetic analysis

The plots of iso-conversional lines in Figures 7–10 were derived from the application of Eqs. (8) and (9) to the TGA data. These include the main steps, such as active pyrolysis, devolatilization, and char combustion. According to the FWO model, activation energy (E), based on Eq. (8), can be determined from the slopes at progressing conversion degrees calculated from the linear plots of $ln\beta$ versus $1/T$ as shown in Figures 8 and 10. Activation energy has also been calculated using the DAEM method using Eq. (9). The linear plots of $ln\frac{\beta}{T^2}$ versus $1/T$ were presented in Figures 7 and 9. In Table 2, the kinetic parameters within a = 0.1–0.7 were presented in this study because of lower correlation values

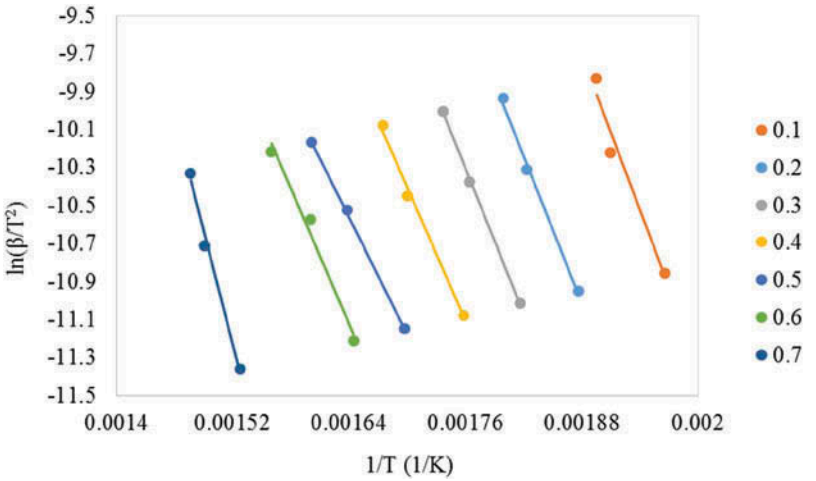

Figure 7. Regression lines to conversion of 10–70% based on the DAEM method for olive pits under oxidative atmosphere.

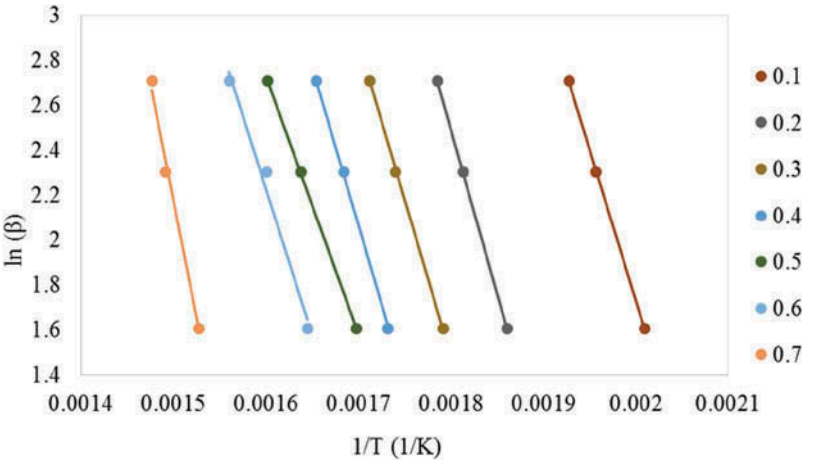

Figure 8. Regression lines to conversion of 10–70% based on the FWO method for plum pits under oxidative atmosphere.

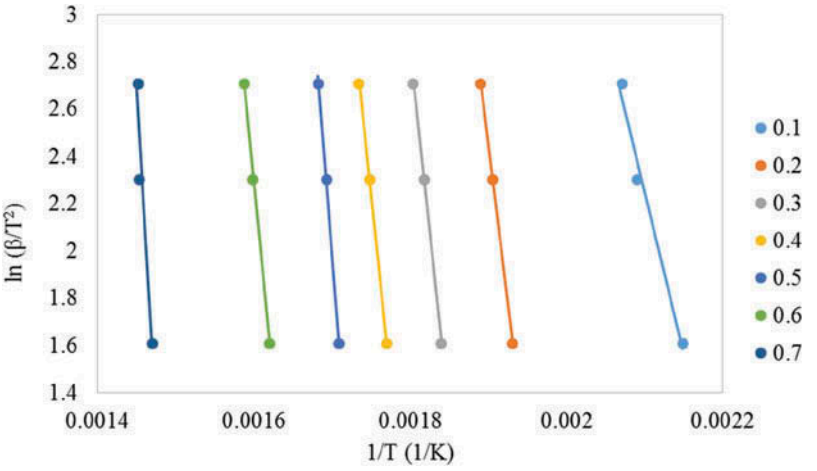

Figure 9. Regression lines to conversion of 10–70% based on the DAEM method for stalk under inert atmosphere.

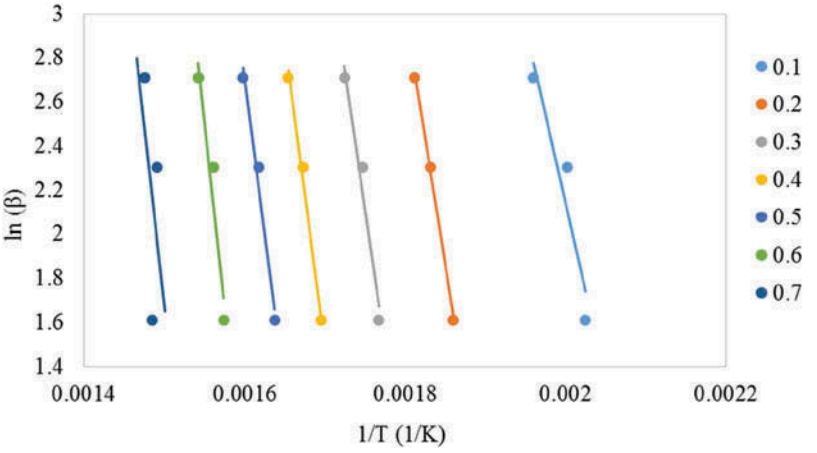

Figure 10. Regression lines to conversion of 10–70% based on the FWO method for marc under inert atmosphere.

obtained at conversion degrees above 0.7 (Ceylan and Topcu, 2014). It was observed that the results for the E obtained from FWO and DAEM methods were similar with a difference below 7% in inert atmosphere and a difference below 8% in oxidation atmosphere for both studied steps (Figure 11). Lopez-Velazquez et al. (2013) reported that the results with deviations lower than 10% between the Friedman and Kissinger–Akahira–Sunose methods validated the reliability of the performed calculations and the excellent predictive power of the direct methods. This indicated that the results calculated by FWO and DAEM methods with differences below 8% were reliable and predictive in this study.

Figures 12–15 show a high dependence of the activation energy on a, which indicated the existence of a complex multi-step mechanism that occurs in the solid state (Damartzis et al., 2011; Slopiecka et al., 2012). For example, the activation energy of plum pits in inert

Table 2. Activation energy for conversion range of 0.1–0.7 using DAEM and FWO methods in an inert atmosphere for all biomass.

Biomass	Conversion (α)	DAEM model E (kJ/mol)	A (s^{-1})	R^2	FWO model E (kJ/mol)	R^2	Difference (%)
Sawdust	0.1	96.41	$9.17 * 10^{08}$	0.99	99.88	0.99	3.60
	0.2	130.33	$3.99 * 10^{11}$	0.99	132.7	0.99	1.79
	0.3	144.62	$3.25 * 10^{12}$	0.99	146.58	0.99	1.34
	0.4	157.51	$2.11 * 10^{13}$	0.99	159.07	0.99	0.98
	0.5	162.74	$2,97 * 10^{13}$	0.99	164.25	0.99	0.92
	0.6	172.63	$1.22 * 10^{14}$	0.99	173.81	0.99	0.68
	0.7	192.54	$3.14 * 10^{15}$	0.98	192.9	0.98	0.19
	Average	150.97			152.74		
	σ	28.83			27.93		
Plum pits	0.1	126.96	$4.95 * 10^{12}$	0.99	128.59	0.99	1.28
	0.2	138.86	$4.96 * 10^{12}$	0.99	140.62	0.99	1.25
	0.3	154.03	$3.46 * 10^{13}$	0.99	155.43	0.99	0.90
	0.4	165.28	$1.06 * 10^{14}$	0.99	166.46	0.99	0.71
	0.5	163.7	$2.58 * 10^{13}$	0.99	165.26	0.99	0.94
	0.6	155.82	$2.24 * 10^{12}$	0.98	158.03	0.97	1.40
	0.7	151.71	$4.50 * 10^{11}$	0.97	154.38	0.96	1.73
	Average	150.91			152.68		
	σ	12.66			12.60		
Peach pits	0.1	130.62	$9.13 * 10^{11}$	0.99	132.75	0.99	1.63
	0.2	130.84	$3.43 * 10^{11}$	0.99	133.25	0.99	1.81
	0.3	134.66	$3.29 * 10^{11}$	0.99	137.17	0.99	1.83
	0.4	140.73	$4.75 * 10^{11}$	0.99	143.2	0.99	1.72
	0.5	141.04	$2.08 * 10^{11}$	0.99	143.78	0.99	1.91
	0.6	145.01	$2.35 * 10^{11}$	0.98	147.78	0.98	1.87
	0.7	114.37	$2.69 * 10^{08}$		119.01	0.75	3.90
	Average	133.90			136.71		
	σ	9.43			8.91		
Olive pits	0.1	162.81	$7.25 * 10^{15}$	0.99	163.00	0.99	0.12
	0.2	162.38	$7.01 * 10^{14}$	0.99	163.08	0.99	0.43
	0.3	168.23	$6.54 * 10^{14}$	0.99	168.97	0.99	0.44
	0.4	166.69	$1.72 * 10^{14}$	0.99	167.77	0.99	0.64
	0.5	166.82	$7.31 * 10^{13}$	0.94	168.15	0.95	0.79
	0.6	153.47	$1.47 * 10^{12}$	0.90	155.83	0.70	1.51
	0.7	82.97	$1.86 * 10^{7}$	0.90	89.38	0.75	7.17
	Average	151.91			153.74		
	σ	28.51			26.61		
Stalk	0.1	173.23	$4.01 * 10^{18}$	0.99	107.18	0.98	38.13
	0.2	214.58	$1.15 * 10^{21}$	0.99	212.24	0.99	1.09
	0.3	246.72	$1.41 * 10^{23}$	0.99	243.19	0.99	1.43
	0.4	252.86	$6.16 * 10^{22}$	0.99	249.38	0.99	1.38
	0.5	334.01	$2.10 * 10^{29}$	0.99	326.82	0.99	2.15
	0.6	270.82	$1.90 * 10^{22}$	0.99	264.26	0.99	2.42
	0.7	435.35	$8.09 * 10^{32}$	0.92	424.65	0.92	2.46
	Average	275.37			261.10		
	σ	79.74			90.72		
Marc	0.1	124.09	$2.53 * 10^{12}$	0.89	125.89	0.90	1.45
	0.2	179.57	$5.84 * 10^{16}$	0.99	179.3	0.99	0.15
	0.3	202.56	$1.09 * 10^{18}$	0.99	201.3	0.99	0.63
	0.4	215.27	$2.38 * 10^{18}$	0.99	214.07	0.99	0.56
	0.5	221.39	$1.76 * 10^{18}$	0.97	220.22	0.96	0.53
	0.6	268.21	$2.70 * 10^{21}$	0.93	265.1	0.93	1.17
	0.7	252.21	$1.17 * 10^{19}$	0.90	250.41	0.72	0.72
	Average	209.04			208.04		
	σ	44.21			42.85		

atmosphere is about 128.59–166.46 kJ/mol and 126.96–165.28 kJ/mol for FWO and DAEM, respectively. Tables 2 and 3 present the average values and deviation standard of kinetic parameters calculated by FWO and DAEM methods. The variation of *E* values

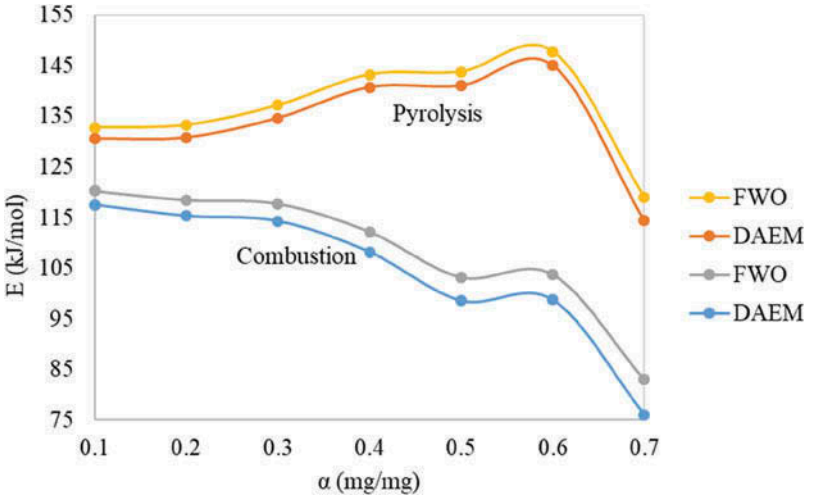

Figure 11. Dependence of the activation energy on the extent of conversion for peach pits.

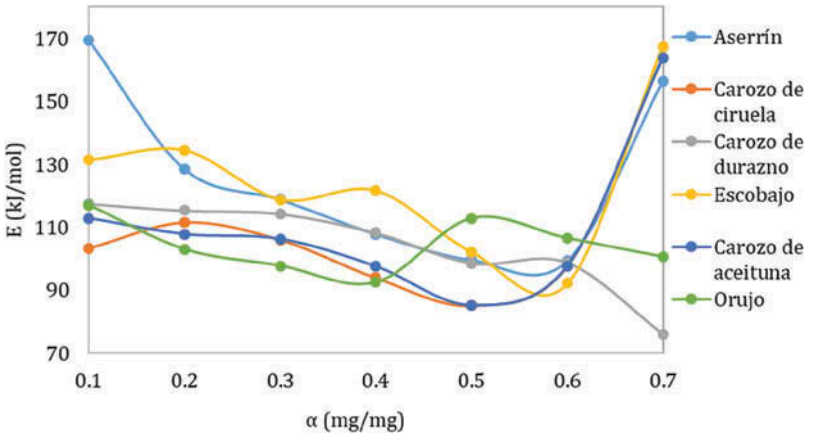

Figure 12. Dependence of the activation energy on the extent of conversion evaluated from the DAEM method for combustion process.

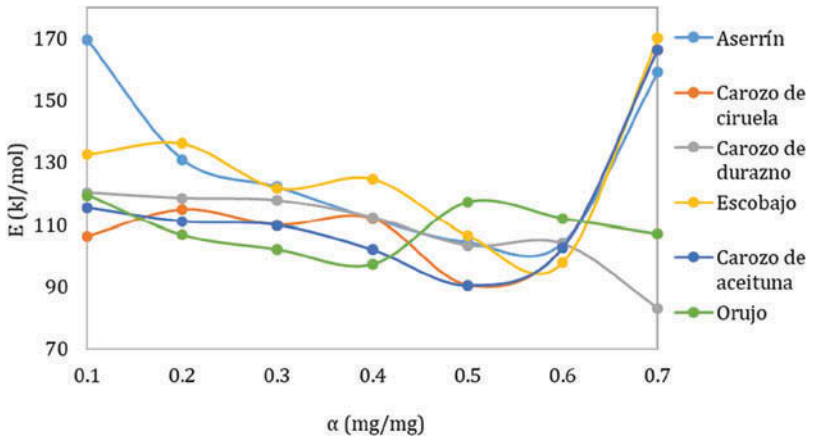

Figure 13. Dependence of the activation energy on the extent of conversion evaluated from the FWO method for combustion process.

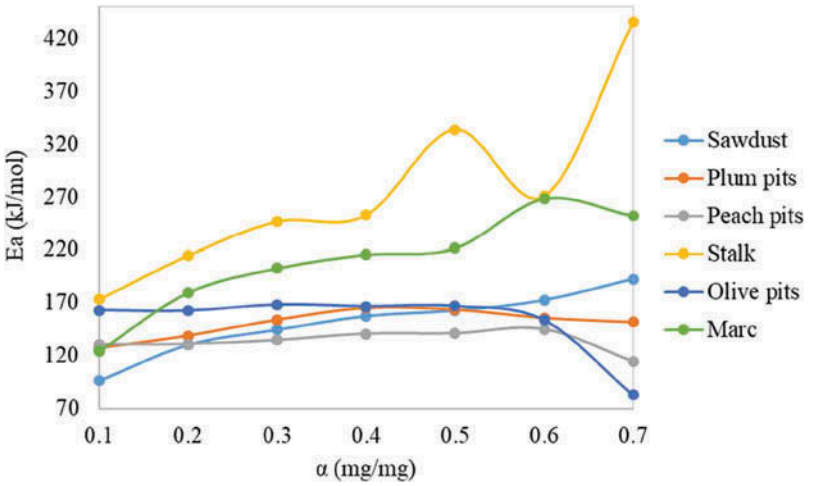

Figure 14. Dependence of activation energy on the extent of conversion evaluated from the DAEM method for pyrolysis process.

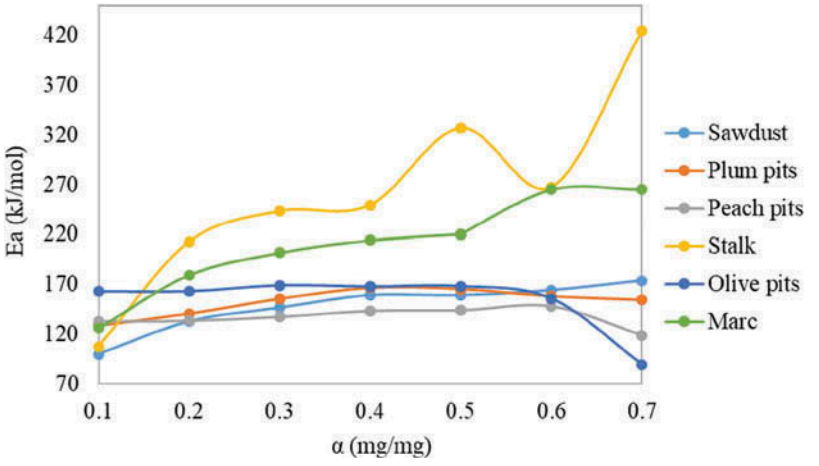

Figure 15. Dependence of activation energy on the extent of conversion evaluated from the FWO method for pyrolysis process.

with progressing conversion might be caused by the change in reaction mechanism (Vyazovkin, 1996). In other words, the reaction mechanism would not stay the same in the whole decomposition process.

Compared with the pyrolysis, the combustion is easily triggered, especially in the second stage, because of the exothermic reaction of organic oxidation (Jiang et al., 2006).

For *a* equals 0.2–0.5, reactions of pyrolysis and combustion were in competition; in fact, in this state, strong disturbances are involved for the determination of the activation energy. During the first stage under oxidative atmosphere (devolatilization), the

Table 3. Activation energy for conversion range of 0.1–0.7 using DAEM and FWO methods in an oxidative atmosphere for all biomass.

		DAEM model			FWO model		
Biomass	Conversion (α)	E (kJ/mol)	A (s^{-1})	R^2	E (kJ/mol)	R^2	Difference (%)
Sawdust	0.1	169.37	$1.71 * 10^{16}$	0.99	169.34	0.99	0.02
	0.2	128.48	$2.52 * 10^{11}$	0.99	130.95	0.99	1.89
	0.3	118.89	$1.27 * 10^{10}$	0.99	122.10	0.99	2.63
	0.4	107.86	$6.10 * 10^{08}$	0.99	111.86	0.99	3.58
	0.5	99.68	$6.59 * 10^{07}$	0.99	104.29	0.99	4.42
	0.6	99.39	$4.74 * 10^{07}$	0.99	104.18	0.99	4.60
	0.7	156.47	$8.61 * 10^{11}$	0.98	158.96	0.98	1.57
	Average	125.73			128.81		
	σ	25.6			24.19		
Plum pits	0.1	103.39	$9.68 * 10^{09}$	0.99	106.31	0.99	2.75
	0.2	111.61	$8.94 * 10^{09}$	0.99	114.77	0.99	2.75
	0.3	106.05	$9.30 * 10^{08}$	0.99	109.82	0.99	3.43
	0.4	94.00	$3.58 * 10^{07}$	0.99	111.86	0.99	15.97
	0.5	85.19	$2.89 * 10^{06}$	0.99	90.56	0.99	5.93
	0.6	97.65	$2.20 * 10^{07}$	0.98	102.68	0.97	4.90
	0.7	163.91	$1.48 * 10^{12}$	0.99	166.32	0.96	1.45
	Average	108.83			114.62		
	σ	23.85			22.34		
Peach pits	0.1	117.50	$5.41 * 10^{10}$	0.99	120.25	0.99	2.29
	0.2	115.31	$1.22 * 10^{10}$	0.99	118.46	0.99	2.66
	0.3	114.28	$4.68 * 10^{09}$	0.99	117.74	0.99	2.94
	0.4	108.21	$6.34 * 10^{08}$	0.99	112.24	0.99	3.59
	0.5	98.59	$5.25 * 10^{07}$	0.99	103.28	0.99	4.54
	0.6	98.76	$2.58 * 10^{07}$	0.98	103.82	0.98	4.87
	0.7	76.10	$8.47 * 10^{04}$	0.80	83.04	0.75	8.36
	Average	104.11			108.40		
	σ	13.46			12.15		
Olive pits	0.1	112.89	$5.49 * 10^{10}$	0.99	115.49	0.99	2.25
	0.2	107.79	$4.49 * 10^{09}$	0.99	111.05	0.99	2.94
	0.3	106.26	$1.37 * 10^{09}$	0.99	109.89	0.99	3.30
	0.4	97.55	$8.93 * 10^{07}$	0.99	101.90	0.99	4.27
	0.5	85.19	$2.88 * 10^{06}$	0.99	90.56	0.95	5.93
	0.6	97.64	$2.20 * 10^{07}$	0.98	102.68	0.70	4.91
	0.7	163.91	$1.48 * 10^{12}$	0.99	166.32	0.75	1.45
	Average	110.18			113.98		
	σ	23.47			22.64		
Stalk	0.1	131.38	$3.49 * 10^{13}$	0.98	132.62	0.98	0.94
	0.2	134.36	$4.52 * 10^{12}$	0.99	136.11	0.99	1.29
	0.3	118.83	$3.30 * 10^{10}$	0.99	121.73	0.99	2.38
	0.4	121.64	$2.48 * 10^{10}$	0.99	124.71	0.99	2.46
	0.5	102.2	$2.83 * 10^{10}$	0.99	106.62	0.99	4.15
	0.6	92.19	$2.78 * 10^{06}$	0.99	97.96	0.99	5.89
	0.7	167.35	$8.62 * 10^{11}$	0.98	170.05	0.92	1.59
	Average	123.99			127.11		
	σ	22.55			21.58		
Marc	0.1	117.03	$2.17 * 10^{11}$	0.88	119.39	0.90	1.98
	0.2	103.01	$1.14 * 10^{09}$	0.99	106.69	0.99	3.45
	0.3	97.78	$1.29 * 10^{08}$	0.99	102.07	0.99	4.20
	0.4	92.49	$1.95 * 10^{07}$	0.99	97.37	0.99	5.01
	0.5	112.91	$5.96 * 10^{08}$	0.98	117.16	0.96	3.63
	0.6	106.54	$2.81 * 10^{07}$	0.99	111.92	0.93	4.81
	0.7	100.65	$2.62 * 10^{06}$	0.99	106.98	0.72	5.92
	Average	104.34			108.80		
	σ	7.91			7.32		

combustion is produced in parallel to pyrolysis, it is faster and takes place at lower temperatures. The oxygen reacts with the solid that is being decomposed before reaching the flame formation (Font et al., 2005).

Tables 4 and 5 show that the mass loss rate maximum (dry basis) in inert atmosphere was lower than oxidative atmosphere at the three heating rates, during the second stage. The *E* values for the thermal decomposition under oxidative atmosphere are about 76.10–169.37 kJ/mol and 83.04–169.34 kJ/mol using DAEM and FWO methods, respectively. Table 6 shows the temperature range of char combustion stage and mass loss rate in an oxidative atmosphere.

Conclusions

The kinetics analysis of agro-industrial wastes were studied using TGA under inert and oxidative atmosphere at different heating rates (5 K/min, 10 K/min, and 15 K/min). The activation energies were calculated using DAEM and FWO model-free methods.

Table 4. Temperature range and mass loss rate of active pyrolysis stage in an inert atmosphere.

	Heating rate	Temperature range	Peak temperature	Mass loss rate maximum
Agro-industrial wastes	β (K/min)	(K)	(K)	(%, s)
Sawdust	5	491–652	605	0.06
	10	473–656	620	0.13
	15	442–702	628	0.19
Plum pits	5	452–671	619	0.04
	10	643–705	632	0.09
	15	452–738	640	0.12
Peach pits	5	501–654	627	0.06
	10	505–671	637	0.10
	15	496–673	646	0.16
Stalk	5	459–638	573	0.03
	10	466–655	578	0.06
	15	455–657	588	0.10
Olive pits	5	459–744	581	0.05
	10	458–758	594	0.10
	15	467–771	604	0.14
Marc	5	469–754	608	0.07
	10	482–768	621	0.06
	15	479–787	623	0.09

Table 5. Temperature range and mass loss rate of devolatilization stage in an oxidative atmosphere.

	Heating rate	Temperature range	Temperature peak	Mass loss rate maximum
Agro-industrial wastes	β (K/min)	(K)	(K)	(%, s)
Sawdust	5	517–604	586	0.10
	10	526–615	601	0.26
	15	534–634	618	0.41
Plum pits	5	503–628	584	0.06
	10	506–636	612	0.13
	15	512–652	633	0.19
Peach pits	5	509–610	585	0.11
	10	519–632	603	0.20
	15	525–646	618	0.23
Stalk	5	461–607	552	0.05
	10	477–603	565	0.10
	15	488–617	580	0.15
Olive pits	5	487–609	577	0.08
	10	505–607	598	0.19
	15	494–629	600	0.28
Marc	5	488–631	561	0.04
	10	501–632	587	0.10
	15	498–642	610	0.14

Table 6. Temperature range and mass loss rate of char combustion stage in an oxidative atmosphere.

	Heating rate	Temperature range	Temperature peak	Mass loss rate maximum
Agro-industrial wastes	β (K/min)	(K)	(K)	(%, s)
Sawdust	5	662–744	708	0.04
	10	687–750	720	0.08
	15	689–479	744	0.022
Plum pits	5	667–760	719	0.18
	10	686–790	737	0.08
	15	699–796	748	0.10
Peach pits	5	678–764	738	0.04
	10	714–785	765	0.08
	15	733–813	779	0.09
Stalk	5	649–760	694	0.04
	10	655–759	729	0.04
	15	665–787	742	0.08
Olive pits	5	637–752	681	0.03
	10	653–772	691	0.05
	15	672–784	707	0.08
Marc	5	656–750	697	0.04
	10	687–798	725	0.08
	15	683–795	759	0.16

The shapes of TG curves of the six materials for pyrolysis are similar to those for combustion. Nevertheless, the biomass weight loss is slower and smaller under inert atmosphere than oxidative atmosphere.

Considering the heating rate influence in the behavior during the thermal decomposition under inert and oxidative atmospheres, it is observed that the temperature range of the different decomposition stages is not affected by the heating rate. When the heating rate increases, the obtained peak in DTG curves is lower, due to a longer time, which is required for the gas to reach equilibrium with the reactor temperature or particles sample as a result of the heat transfer restrictions. The weight loss is not affected when the heating rate is varied.

It was found that, at heating rates used, the activation energy was not linearly dependent on conversion for both studied thermal processes, pyrolysis, and combustion. Activation energy of pyrolysis was higher than the devolatilization stage of combustion in all cases; they were dependent upon the conversion and were in the ranges of 82.97–435.35 kJ/mol for the pyrolysis and 76.1–169.37 kJ/mol for the combustion. During this stage, under oxidative atmosphere, the combustion is produced in parallel to pyrolysis; the oxygen reacts with the remaining solid.

The kinetic analysis was carried out for the active pyrolysis (decomposition under inert atmosphere), devolatilization, and char combustion (decomposition under oxidative atmosphere), using FWO and DAEM methods. The E values obtained from both methods were similar, considering that the obtained results are reliable and predictive.

The variation of E values with a, indicate the existence of a complex multi-step mechanism that occurs in the solid state.

References

Abdullah, H., and Wu, H. 2009. Biochar as a fuel: 1. Properties and grindability of biochars produced from the pyrolysis of mallee wood under slow-heating conditions. *Energy Fuels*, **23**, 4174–4181.

Abed, I., Paraschiv, M., Loubar, K., Zagrouba, F., and Tazerout, M. 2012. Thermogravimetric investigation and thermal conversion kinetics of typical North African and middle eastern lignocellulosic wastes. *BioResources*, **7**(1), 1200–1220.

Ahmad, M., Rajapaksha, A., Lim, J., Zhang, M., Bolan, N., Mohan, D., Vithanage, M., Lee, S., Ok, Y. 2014. Biochar as a sorbent for contaminant management in soil and water: A review. *Chemosphere*, **99**, 19–23.

Aouad, A., Bilali, L., Benchanâa, M., and Mokhlisse, A. 2002. Kinetic aspect of thermal decomposition of natural phosphate and its kerogen: Influence of heating rate and mineral matter. *J. Therm. Anal. Calorim.*, **67**, 733–743.

Bhavanam, A., and Sastry, R.C. 2014. Kinetic study of solid waste pyrolysis using distributed activation energy model. *Bioresour. Technol.*, **178**, 126–131.

Biney, P., Gyamerah, M., Shen, J., and Menezes, B. 2015. Kinetics of the pyrolysis of arundo, sawdust, corn stover and switch grass biomass by thermogravimetric analysis using a multi-stage model. *Bioresour. Technol.*, **179**, 113–122

Borah, D., Barua, M., and Baruah, M.K. 2005. Dependence of pyrite concentration on kinetics and thermodynamics of coal pyrolysis in non-isothermal systems. *Fuel Process. Technol.*, **86**, 977–993.

Cai, J., Wu, W., and Liu, R. 2014. An overview of distributed activation energy model and its application in the pyrolysis of lignocellulosic biomass. *Renewable Sustainable Energy Rev.*, **36**, 236–246.

Carlson, T.R., Cheng, Y.T., Jae, J., and Huber, G.W. 2011. Production of green aromatics and olefins by catalytic fast pyrolysis of wood sawdust. *Energy Environ. Sci.*, **4**, 145–161.

Carpenter, D., Westover, T.L., Czernik, S., and Jablonski, W. 2014. Biomass feedstocks for renewable fuel production: a review of the impacts of feedstock and pretreatment on the yield and product distribution of fast pyrolysis bio-oils and vapors. *Green Chem.*, **16**, 384–406.

Ceylan, S., and Topcu, Y. 2014. Pyrolysis kinetics of hazelnut husk using thermogravimetric analysis. *Bioresour. Technol.*, **156**, 182–188.

Channiwala, S.A., and Parikh, P.P. 2002. Unified correlation for estimating HHV of solid, liquid and gaseous fuels. *Fuel*, **81**(8), 1051–1063.

Chouchene, A., Jeguirim, M., Khiari, B., Zagrouba, F., and Trouvé, G. 2010. Thermal degradation of olive solid waste: Influence of particle size and oxygen concentration. *Resourc., Conserv. Recycl.*, **54**, 271–277.

Crnkovic, P.M., Koch, C., Ávila, I., Mortari, D.A., Cordoba, A.M., and Moreira dos Santos, A. 2012. Determination of the activation energies of beef tallow and crude glycerin combustion using thermogravimetry. *Biomass Bioenergy*, **44**, 8–16.

Damartzis, T., Vamvuka, D., Sfakiotakis, S., and Zabaniotou, A. 2011. Thermal degradation studies and kinetic modeling of cardoon (*Cynara cardunculus*) pyrolysis using thermogravimetric analysis (TGA). *Bioresour. Technol.*, **102**, 6230–6238.

Daouk, E., Van de Steene, L., Paviet, F., and Salvador, S. 2015. Thick wood particle pyrolysis in an oxidative atmosphere. *Chem. Eng. Sci.*, **126**, 608–615.

Demirbas, A. 2004. Effects of temperature and particle size on bio-char yield from pyrolysis of agricultural residues. *J. Anal. Appl. Pyrolysis*, **72**(2), 243–248.

Demirbas, A., and Arin, G. 2002. An overview of biomass pyrolysis. *Energy Sources*, **24**(5), 471–482.

Department of Minerals and Energy. 2003. White Paper on Renewable Energy. Department of Minerals and Energy, Republic of South Africa.

Di Blasi, C. 2008. Modeling chemical and physical process of wood and biomass pyrolysis. *Prog. Energy Combust. Sci.*, **34**, 47–90.

Doyle, C.D. 1961. Estimating thermal stability of experimental polymers by empirical thermogravimetric analysis. *Anal. Chem.*, **33**, 77–79.

Dufour, A., Weng, J., Jia, L., Tang, X., Sirjean, B., Fournet, R., et al. 2013. Revealing the chemistry of biomass pyrolysis by means of tunable synchrotron photoionisation–mass spectrometry. *RSC Adv.*, **3**, 4786–4792.

Ericsson, K., and Werner, S. 2016. The introduction and expansion of biomass use in Swedish district heating systems. *Biomass Bioenergy*, **94**, 57–65.

Fernandez, A., Saffe, A., Mazza, G., and Rodriguez, R. 2017. Kinetic analysis of regional agro-industrial waste combustion. *Biofuels*, **8**(1), 71–80.
Fernandez, A., Saffe, A., Pereyra, R., Mazza, G., and Rodriguez, R. 2016. Kinetic study of regional agro-industrial wastes pyrolysis using non-isothermal TGA analysis. *Appl. Therm. Eng.*, **106**, 1157–1164.
Fiori, L., Valbusa, M., Lorenzi, D., and Fambri, L. 2012. Modeling of the devolatilization kinetics during pyrolysis of grape residues. *Bioresour. Technol.*, **103**, 389–397.
Font, R., Fullana, A., and Conesa, J. 2005. Kinetic models for the pyrolysis and combustion of two types of sewage sludge. *J. Anal. Appl. Pyrolysis*, **74**, 429–438.
Gao, W., Chen, K., Xiang, Z., Yang, F., Zeng, J., Li, J., Yang, R., Rao, G., Tao, H. 2013. Kinetic study on pyrolysis of tobacco residues from the cigarette industry. *Ind. Crops Prod.*, **44**, 152–157.
George, A., Morgan, T., and Kandiyoti, R. 2014. Pyrolytic reactions of lignin within naturally occurring plant matrices: Challenges in biomass pyrolysis modeling due to synergistic effects energy. *Fuels*, **28**, 6918–6927.
Grammelis, P., Basinas, P., Malliopoulou, A., and Sakellaropoulos, G. 2009. Pyrolysis kinetics and combustion characteristics of waste recovered fuels. *Fuel*, **88**(1), 195–205.
INTA (Instituto Nacional de Tecnología Agropecuaria). 2015. *Informes Técnicos*. INTA, Argentina. ISSN 22508481.
Jahirul, M.I., Rasul, M.G., Chowdhury, A.A., and Ashwath, N. 2012. Biofuels production through biomass pyrolysis—A technological review. *Energies*, **5**, 4952–5001.
Jeguirim, M., and Trouvé, G. 2009. Pyrolysis characteristics and kinetics of Arundo donax using thermogravimetric analysis. *Bioresour. Technol.*, **100**, 4026–4031.
Jiang, X.M., Han, X.X., and Cui, Z.G. 2006. Mechanism and mathematical model of Huadian oil shale pyrolysis. *J. Therm. Anal. Calorim.*, **86**, 457–462.
Jung, C., Park, J., Lim, K.H., Park, S., Heo, J., Her, N., et al. 2013. Adsorption of selected endocrine disrupting compounds and pharmaceuticals on activated biochars. *J. Hazard Mater.*, **263**, 702–710.
Kök, M.V. 1998. Temperature-controlled combustion and kinetics of different rank coal samples. *J. Therm. Anal. Calorim.*, **79**, 175–180.
Kök, M.V. 2003. Coal pyrolysis: Thermogravimetric study and kinetic analysis. *Energy Sources*, **25**, 1007–1014.
Kök, M.V., and Karacan, O. 1998. Pyrolysis analysis and kinetics of crude oils. *J. Therm. Anal. Calorim.*, **52**, 781–788.
Kök, M.V., and Pamir, R. 2003. Pyrolysis kinetics of oil shales determined by DSC and TG/DTG. *Oil Shale*, **20**, 57–68.
Lehmann, J. 2007. A handful of carbon. *Nature*, **447**, 143–144.
Lestander, T.A., and Rhén, C. 2005. Multivariate NIR spectroscopy models for moisture, ash and calorific content in biofuels using bi-orthogonal partial least squares regression. *Analyst*, **130**(8), 1182–1889.
Lili, L., Nan, Z., Xiaobin, F., Mingfei, S., and Song, Q. 2013. Thermogravimetric and kinetic analysis of Spirulina wastes under nitrogen and air atmospheres. *Bioresour. Technol.*, **140**, 152–157.
Lopez-Velazquez, M.A., Santes, V., Balmaseda, J., and Torres-Garcia, E. 2013. Pyrolysis of orange waste: A thermo-kinetic study. *J. Anal. Appl. Pyrolysis*, **99**, 170–177.
Manya, J.J. 2012. Pyrolysis for biochar purposes: A review to establish current knowledge gaps and research needs. *Environ. Sci. Technol.*, **46**, 7939–7954.
Meszaros, E., Varhegyi, G., Jakab, E., and Marosvolgyi, B. 2004. Thermogravimetric and reaction kinetic analysis of biomass samples from an energy plantation. *Energy Fuels*, **18**, 497–507.
Mettler, M.S., Vlachos, D.G., and Dauenhauer, P.J. 2012. Top ten fundamental challenges of biomass pyrolysis for biofuels. *Energy Environ. Sci.*, **5**, 7797–7809.
Mitchell, C., and Connor, P.M. 2004. Renewable energy policy in the UK 1990–2003. *Energy Policy*, **32**(17), 1935–1947.
Nunes, L.J.R., Matias, J.C.O., and Catalão, J.P.S. 2017. Biomass in the generation of electricity in Portugal: A review. *Renewable Sustainable Energy Rev.*, **71**, 373–378.

Parikh, J., Channiwala, S.A., and Ghosal, G.K. 2005. A correlation for calculating HHV from proximate analysis of solid fuels. *Fuel*, **84**, 487–494.

Paulsen, A., Hough, B., Williams, C., Teixeira, A., Schwartz, D., Pfaendtner, J., and Dauenhauer, P. 2014. Fast pyrolysis of wood for biofuels: Spatiotemporally resolved diffuse reflectance in situ spectroscopy of particles. *ChemSusChem*, 765–776.

Prasad, L., Subbarao, P.M.V., and Subrahmanyam, J.P. 2014. Pyrolysis and gasification characteristics of Pongamia residue (de-oiled cake) using thermogravimetry and downdraft gasifier. *Appl. Therm. Eng.*, **63**, 379–386.

Quirino, W., Vale, A., Andrade, A., Abreu, V., and Azevedo, A. 2005. Poder calorífico da madeira e de materiais lignocelulósicos. *Revista da Madeira*, **89**, 100–106.

Sanchez-Silva, L., López-González, D., García-Minguillan, A.M., and Valverde, J.L. 2013. Pyrolysis, combustion and gasification characteristics of Nannochloropsis gaditana microalgae. *Bioresour. Technol.*, **130**, 321–331.

Senelwa, K., and Sims, R.E.H. 1999. Fuel characteristics of short rotation forest biomass. *Biomass Bioenergy*, **17**, 127–140.

Slopiecka, K., Bartocci, P., and Fantozzi, F. 2012. Thermogravimetric analysis and kinetic study of poplar wood pyrolysis. *Appl. Energy*, **97**, 491–497.

Talmadge, M., Baldwin, R., Biddy, M., McCormick, R., Beckham, G., Ferguson, G., Czernik, S., Magrini-Bair, K., Foust, T., Metelski, P., Hetrick, C., and Nimlos, M. 2014. A perspective on oxygenated species in the refinery integration of pyrolysis oil. *Green Chem.*, **16**, 407–453.

Tang, Y.T., Ma, X.Q., and Lai, Z.Y. 2011. Thermo-gravimetric analysis of the combustion of microalgae and microalgae blended with waste in N_2/O_2 and CO_2/O_2 atmospheres. *Bioresour. Technol.*, **102**, 1879–1885.

Valente, M., Brillard, A., Schönnenbeck, C., and Brilhac, J. 2015. Investigation of grape marc combustion using thermogravimetric analysis: Kinetic modeling using an extended independent parallel reaction (EIPR). *Fuel Process. Technol.*, **131**, 297–303.

Vand, V. 1943. A theory of the irreversible electrical resistance changes of metallic films evaporated in vacuum. *Proc. Phys. Soc.*, **55**(3), 222.

Venkatesh, M., Ravi, P., and Tewari, S.P. 2013. Isoconversional kinetic analysis of decomposition of nitroimidazoles: Friedman method vs Flynn–Wall–Ozawa method. *J. Phys. Chem. A*, **117**, 10162–10169.

Volpe, R., Bermudez Menendez, J.M., Ramirez Reina, T., Messineo, A., and Millan, M. 2017. Evolution of chars during slow pyrolysis of citrus waste. *Fuel Process. Technol.*, **158**, 255–263.

Volpe, R., Messineo, A., and Millan, M. 2016. Carbon reactivity in biomass thermal breakdown. *Fuel*, **183**, 139–144.

Vyazovkin, S. 1996. A unified approach to kinetic processing of nonisothermal data. *Int. J. Chem. Kinet.*, **28**, 95–101.

Vyazovkin, S., Burnhamb, A.K., Criado, J.M., Pérez-Maqueda, L.A., Popescu, C., and Sbirrazzuoli, N. 2011. ICTAC kinetics committee recommendations for performing kinetic computations on thermal analysis data. *Thermochim. Acta*, **520**, 1–19.

Wang, S., Lin, H., Ru, B., Dai, G., Wang, X., Xiao, G., and Luo, Z. 2016. Kinetic modeling of biomass components pyrolysis using a sequential and coupling method. *Fuel*, **185**(1), 763–771.

Yang, H., Yan, R., Chen, H., Lee D., and Zheng, C. 2007. Characteristics of hemicellulose, cellulose and lignin pyrolysis. *Fuel*, **86**, 1781–1788.

Zhang, L., Liu, R., Yin, R., and Mei, Y. 2013. Upgrading of bio-oil from biomass fast pyrolysis in China: A review. *Renewable Sustainable Energy Rev.*, **24**, 66–72.

Zheng, G., and Kozi, J.A. 2000. Thermal events occurring during the combustion of biomass residue. *Fuel*, **79**, 181.